Research Article | Vol. 30, No. 19 / 12 Sep 2022 / Optics Express 33664

Optics EXPRESS

On the frequency spanning of SPM-enabled spectral broadening: analytical solutions

JINGSHANG WANG,[1,2] RUNZHI CHEN,[1,2] AND GUOQING CHANG[1,2,3,*]

[1]*Beijing National Laboratory for Condensed Matter Physics, Institute of Physics, Chinese Academy of Sciences, Beijing 100190, China*
[2]*University of Chinese Academy of Sciences, Beijing 100049, China*
[3]*Songshan Lake Materials Laboratory, Dongguan, Guangdong 523808, China*
[*]*guoqing.chang@iphy.ac.cn*

Abstract: We present an analytical treatment of ultra-short pulses propagating in an optical fiber in the strong nonlinearity regime, in which the interaction between self-phase modulation (SPM) and group-velocity dispersion (GVD) substantially broadens the input spectrum. Supported by excellent agreement with the simulation results, these analytical solutions provide a convenient and reasonable accurate estimation of the peak position of the outermost spectral lobes as well as the full width at half maximum of the broadened spectrum. We show that our unified solutions are valid for either Gaussian pulse or hyperbolic secant pulse propagating inside an optical fiber with positive or negative GVD. Our findings shed light on the optimization of SPM-enabled spectral broadening in various applications.

1. Introduction

As an input transform-limited pulse propagates inside an optical fiber, the strong Kerr nonlinearity results in self-phase modulation (SPM) of the propagating pulse [1]. If the fiber has positive group-velocity dispersion (GVD), SPM causes a spectral broadening and thus the pulse develops a positive chirp; removing the chirp by a grating-pair or chirped mirrors generates compressed pulses with the duration much shorter than the initial input pulse [2,3]. To date, spectral broadening via fiber-optic SPM followed by a dechirping device has become a standard technology for nonlinear pulse compression [4]. Such a SPM-enabled spectral broadening can also be used for pulse compression in a fiber with negative GVD. In this scenario, the input pulse may experience duration reduction due to higher-order soliton self-compression [5]. Besides pulse compression, SPM-enabled spectral broadening in optical fibers found wide applications in pulse regeneration [6–12], ultrafast optical signal processing and measurement [13–15], and low-noise supercontinuum generation [16–21]. For a transform-limited pulse of bell-shape, SPM broadens the input spectrum and, at the early broadening state, the spectrum features well-separated spectral lobes; using optical bandpass filters to select the leftmost or rightmost spectral lobes produces nearly transform-limited pulses [22]. Varying the coupled pulse energy into the fiber, the peak wavelength of the leftmost/rightmost spectral lobes can be continuously tuned. Such an SPM-enabled spectral selection (SESS) allowed generation of ~100-fs pulses tunable from 825 nm to 1210 nm based on an Yb-fiber ultrafast laser at 1030 nm [22]. We further applied this method to an Er-fiber laser and the resulting SESS source was tunable from 1300 nm to 1700nm [23,24].

Due to the complicated interaction between SPM and GVD in the strong nonlinearity regime, current investigation of SPM-enabled spectral broadening mainly relies on carefully designed experiments and detailed numerical simulation by solving the nonlinear Schrödinger equation (NLSE). For example, we applied particle swarm optimization method to SESS and found that SESS in an optical fiber with the optimized dispersion can deliver SESS pulses tunable in one octave wavelength range and the conversion efficiency can be as high as 80% [25]. In this paper,

#466033 https://doi.org/10.1364/OE.466033
Journal © 2022 Received 6 Jun 2022; revised 21 Jul 2022; accepted 7 Aug 2022; published 29 Aug 2022

Optics EXPRESS

we present an analytical treatment to the spectral broadening of an optical pulse experiencing both SPM and GVD (positive or negative). We approximate the pulse during the propagation by a Gaussian pulse with the duration and B integral varying with the propagating distance. By incorporating effect of SPM into a properly defined lumped parameter, we find the expression for pulse duration and B integral, which in turn allows us to obtain closed-form analytical solutions to quantify the SPM-enabled spectral broadening.

2. Analytical results on SESS with pure SPM

We first consider spectral broadening by pure SPM, which is described by the following simple equation

$$i\frac{\partial U(z,T)}{\partial z} = -\gamma P_0 |U(z,T)|^2 U(z,T), \tag{1}$$

where $U(z,T)$ represents the normalized amplitude, γ is the Kerr-nonlinearity parameter, and P_0 is the peak power. Equation (1) has the analytical solution

$$U(z,T) = U(0,T)exp[-i\varphi_{Nl}(z,T)], \tag{2}$$

where $\varphi_{Nl}(z,T) = B|U(0,T)|^2$ accounts for the accumulated nonlinear phase. $B = \gamma P_0 z$ is known as B integral. Equation (2) shows that pure SPM does not change the pulse profile while introducing a time-dependent instantaneous frequency $\delta\omega(T) = -d\varphi_{Nl}/dT$, a phenomenon called chirp. For an input transform-limited pules, such a SPM-induced chirp corresponds to spectral broadening of the pulse in the frequency domain. For example, we show in Fig. 1 the broadened spectrum [blue line in Fig. 1(c)] of a Gaussian pulse [Fig. 1(a)] for B=6π. Compared with the input spectrum [black curve in Fig. 1(c)], pure SPM broadens the optical spectrum by a factor of 20 and the broadened spectrum consists of six well-isolated spectral lobes with the two outermost spectral lobes (OSLs) being much stronger than the others. When implementing SESS, a suitable bandpass filter is used to filter the rightmost (or leftmost) spectral lobe, which leads to nearly transform-limited pulse [red curve in Fig. 1(d)]. Because the OSL has a bandwidth 3 times larger than the input spectrum, the resulting SESS pulse has a duration of 2.6 (0.6 versus 1.6) times shorter than the input Gaussian pulse.

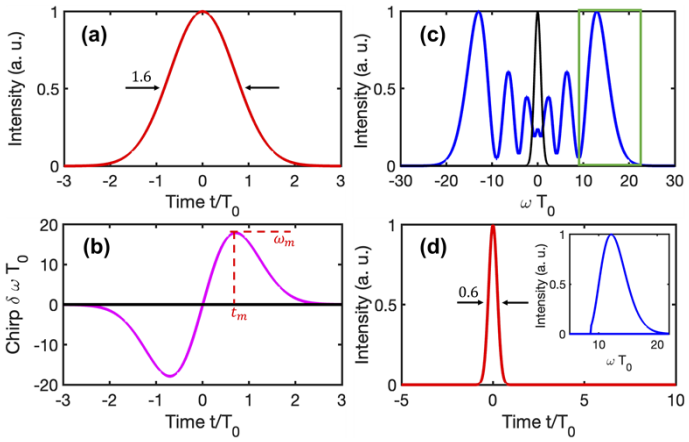

Fig. 1. Spectral broadening by pure SPM for an input transform-limited Gaussian pulse with $B = 6\pi$. (a) Gaussian pulse intensity profile, (b) Normalized chirp, (c) Broadened spectrum, (d) SESS pulse and filtered spectrum (inset).

Apparently, the peak frequencies of the two OSLs determine the frequency tuning range of the resulting SESS pulses. In 2018, Finot *et al.* analyzed the pattern of a broadened spectrum

Optics EXPRESS

resulting from pure SPM for different types of input pulses and obtained analytical expressions for calculating the OSL peak frequency [26]. For an input transform-limited Gaussian pulse $U(0,T) = exp[-T^2/(2T_0^2)]$, they showed that, at the time $t_m = T_0/\sqrt{2}$ [Fig. 1(b)], the instantaneous frequency reaches the maximum value

$$\omega_m = \sqrt{2}e^{-\frac{1}{2}}\frac{B}{T_0}. \tag{3}$$

The OSL peak frequency relative to the center frequency is connected to ω_m by [26]

$$\omega_P \simeq \omega_m - \frac{\pi^{\frac{2}{3}}}{2}\frac{\omega_m^{\frac{1}{3}}}{T_0^{\frac{2}{3}}} \simeq \omega_m\left(1 - 1.19B^{-\frac{2}{3}}\right). \tag{4}$$

Finot *et al.* also showed that, for hyperbolic secant pulse $U(0,T) = \mathrm{sech}(T/T_0)$, the maximum instantaneous frequency (MIF) and the OSL peak frequency are given by

$$\omega_m = \frac{4B}{3\sqrt{3}T_0}, \tag{5}$$

$$\omega_P \simeq \omega_m - \frac{\pi^{\frac{2}{3}}}{2}\frac{\omega_m^{\frac{1}{3}}}{T_0^{\frac{2}{3}}} \simeq \omega_m\left[1 - 1.28B^{-\frac{2}{3}}\right]. \tag{6}$$

Figure 2(a) depicts the spectral broadening of an input transform-limited Gaussian pulse as a function of B integral. The two lines represent the normalized MIF, $\omega_m T_0$ (red line), and the OSL peak frequency, $\omega_P T_0$ (black line). To make a direct comparison, we plot in Fig. 2(b) the normalized OSL peak frequency given by simulations (blue squares) and by Eq. (4) (blue curve)

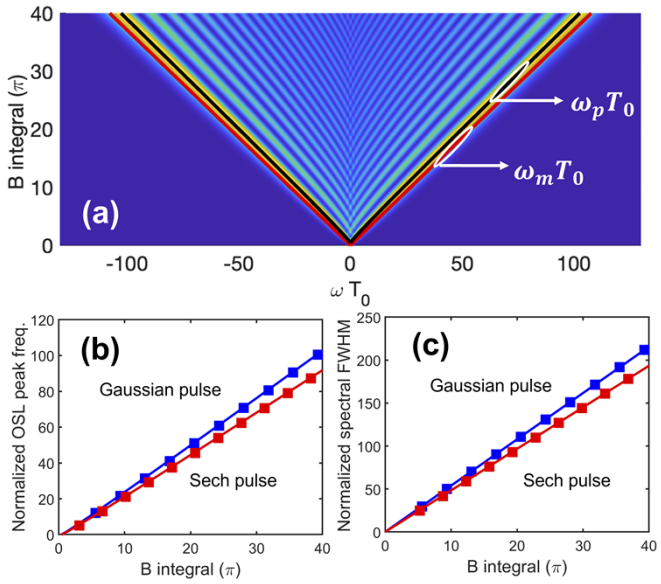

Fig. 2. (a) Spectral broadening versus B integral. The normalized MIF $\omega_m T_0$ and the normalized OSL peak frequency $\omega_p T_0$ are plotted as red curve and black curve, respectively. (b) Normalized OSL peak frequency and (c) Normalized spectral FWHM given by simulation and analytical solution for Gaussian pulse (blue squares versus blue curves) and hyperbolic secant pulse (red squares versus red curves), respectively.

Optics EXPRESS

as a function of B integral. Also plotted in Fig. 2(b) are the simulation results (red squares) and the analytical prediction (red curve) by Eq. (6) for the input being a transform-limited hyperbolic secant pulse. Clearly Eqs. (4)(6) provide an excellent prediction of OSL peak frequency. According to Ref. [26], ω_m denotes the MIF. In this paper we point out that $2\omega_m$ can serve as a good estimation of the full width at half maximum (FWHM) of the broadened spectrum. This is evidenced by the nearly perfect agreement for the normalized FWHM obtained by simulation results [solid squares in Fig. 2(c)] and by $2\omega_m T_0$ [blue and red curves in Fig. 2(c)] for both Gaussian pulse and hyperbolic secant pulse.

3. SPM-enabled spectral broadening with GVD

The analytical results [i.e., Eqs. (3-6)] are valid for estimating the OSL peak frequency and FWHM of an optical spectrum broadened by pure SPM. In reality, fiber GVD needs to be taken into account, and thus Eq. (1) is replaced by the famous NLSE [27]:

$$i\frac{\partial U}{\partial z} = \frac{\beta_2}{2}\frac{\partial^2 U}{\partial T^2} - \gamma P_0|U|^2 U. \tag{7}$$

The associated complicated interaction between GVD and SPM gives rise to well-known nonlinear phenomena, such as optical wave-breaking for positive GVD and higher-order soliton compression for negative GVD. Dispersion length $L_d = T_0^2/\beta_2$ and nonlinear length $L_{NL} = 1/(\gamma P_0)$ are defined to quantify the strength of GVD and SPM. Except under some special conditions, this NLSE cannot be solved analytically. Nevertheless, many researchers tried to obtain analytical results using some approximations to reveal the physics behind the complicated nonlinear interaction. For example, Eq. (7) has been extensively analyzed for weak nonlinearity (i.e., $L_d \ll L_{NL}$) with a focus on the pulse temporal evolution since the spectral width only slightly changes [28–30]. On the other hand, substantial spectral broadening requires strong nonlinearity (i.e., $L_{NL} \ll L_d$), and many researchers have investigated Eq. (7) under this condition as well to gain some analytical insights [18,31–35]. In 2018, Zheltikov presented a closed-form analytical description of the spectral width for the early stage of SPM-enabled spectral broadening with the presence of positive or negative GVD [35]. More specifically, he assumed that an input Gaussian pulse maintains its pulse shape during the early stage of spectral broadening. To analytically estimate the z-dependent pulse duration, the effect of SPM is represented by a lumped chirp parameter α_0 [35]; that is, the initial pulse is given by

$$U(0,T) = exp\left(-\frac{T^2}{2T_0^2} - i\alpha_0 T^2\right). \tag{8}$$

Then the pulse propagates linearly in the fiber with its duration only affected by GVD:

$$T(z) = T_0\left[(1-\alpha_0\beta_2 z)^2 + \left(\frac{z}{L_d}\right)^2\right]^{\frac{1}{2}}. \tag{9}$$

In Ref. [35], Zheltikov assumed $\alpha_0 = -2\gamma P_0 z/T_0^2$, and it follows that

$$T(z) = T_0\left[\left(1 + \frac{2\mathrm{sgn}(\beta_2)|\beta_2|\gamma P_0 z^2}{T_0^2}\right)^2 + \left(\frac{z}{L_d}\right)^2\right]^{\frac{1}{2}}. \tag{10}$$

By neglecting $(z/L_d)^2$ and z^4 terms in Eq. (10), Zheltikov obtained the following expression for the z-dependent pulse duration:

$$T(z) = T_0\left[1 + \frac{4\mathrm{sgn}(\beta_2)z^2}{L_d L_{NL}}\right]^{\frac{1}{2}} = T_0\left[1 + \mathrm{sgn}(\beta_2)\left(\frac{z}{L_c}\right)^2\right]^{\frac{1}{2}}. \tag{11}$$

Optics EXPRESS

$L_c = \sqrt{L_{NL}L_d}/2$ defines a characteristic length, which Zheltikov identified as the propagation distance corresponding to the maximum pulse compression for negative GVD [35]. Then the amount of spectral broadening is estimated to be

$$\Delta\omega(z) = \gamma \int_0^z \frac{P(z)}{T(z)} dz. \tag{12}$$

Considering $P(z)T(z) = P_0T_0$, Zheltikov obtained following analytical expressions for calculating the spectral broadening:

$$\Delta\omega(z) \approx \frac{\gamma P_0}{T_0} \int_0^z \left[1 + sgn(\beta_2)\left(\frac{z}{L_c}\right)^2\right]^{-1} dz = \begin{cases} \frac{1}{T_0}\frac{L_c}{L_{NL}}\tan^{-1}\left(\frac{z}{L_c}\right), \beta_2>0 & (13) \\ \frac{1}{T_0}\frac{L_c}{L_{NL}}\tanh^{-1}\left(\frac{z}{L_c}\right), \beta_2<0 & (14) \end{cases}$$

Motivated by Ref. [26,35], we adopt a different method to obtain analytical description of SPM-enabled spectral broadening with a focus on estimating the OSL peak frequency and the spectral FWHM. We make a further assumption that

$$U(z,T) \propto exp\left[-\frac{T^2}{2T(z)^2}\right] exp\left\{iB(z)exp\left[-\frac{T^2}{T(z)^2}\right]\right\}. \tag{15}$$

Following the approach in Ref. [26], we only need to determine the B integral $B(z)$, and the pulse duration $T(z)$, in order to calculate the MIF ω_m, and the OSL peak frequency ω_P. To estimate $T(z)$, instead of the chirp defined by $\alpha_0 = -2\gamma P_0 z/T_0^2$ in Ref. [36], we assume

$$\alpha_0 = -\frac{1}{\kappa^2}\frac{2\gamma P_0 z}{T_0^2}, \tag{16}$$

where κ is later determined by matching the analytical solutions and the simulation results. Consequently Eq. (11) is modified to estimate the z-dependent pulse duration:

$$T(z) \approx T_0\left[1 + \frac{\mathrm{sgn}(\beta_2)z^2}{(\kappa L_c)^2}\right]^{\frac{1}{2}}. \tag{17}$$

The B integral is given by

$$B(z) = \gamma \int_0^z P(z)dz = \gamma \int_0^z \frac{P_0T_0}{T(z)} dz = \gamma P_0 \int_0^z \left[1 + \frac{\mathrm{sgn}(\beta_2)z^2}{(\kappa L_c)^2}\right]^{-\frac{1}{2}} dz. \tag{18}$$

For positive GVD, it follows that

$$B(z) = \gamma P_0 \int_0^z \left[1 + \frac{z^2}{(\kappa L_c)^2}\right]^{-\frac{1}{2}} dz = \frac{\kappa L_c}{L_{NL}}\sinh^{-1}\left(\frac{z}{\kappa L_c}\right) = \frac{\kappa N}{2}\sinh^{-1}\left(\frac{z}{\kappa L_c}\right) \tag{19}$$

where $N = \sqrt{L_d/L_{NL}}$ is the soliton number that quantifies the relative strength of dispersion and nonlinearity. Similarly, for negative GVD we have

$$B(z) = \gamma P_0 \int_0^z \left[1 - \frac{z^2}{(\kappa L_c)^2}\right]^{-\frac{1}{2}} dz = \frac{\kappa N}{2}\sin^{-1}\left(\frac{z}{\kappa L_c}\right). \tag{20}$$

Optics EXPRESS

3.1. Spectral broadening of transform-limited Gaussian pulse

For an input transform-limited Gaussian pulse, we use Eq. (3) to estimate the MIF:

$$\omega_m(z) = \sqrt{2}e^{-\frac{1}{2}}\frac{B(z)}{T(z)} = \begin{cases} \frac{e^{-\frac{1}{2}}\kappa N}{\sqrt{2}T_0}\sinh^{-1}\left(\frac{z}{\kappa L_c}\right)\left[1+\frac{z^2}{(\kappa L_c)^2}\right]^{-\frac{1}{2}}, \ \beta_2>0 \quad (21) \\ \frac{e^{-\frac{1}{2}}\kappa N}{\sqrt{2}T_0}\sin^{-1}\left(\frac{z}{kL_c}\right)\left[1-\frac{z^2}{(\kappa L_c)^2}\right]^{-\frac{1}{2}}, \ \beta_2<0 \quad (22) \end{cases}$$

According to Eq. (4), the OSL peak frequency follows

$$\omega_P(z) \simeq \omega_m - \frac{\pi^{\frac{2}{3}}}{2}\frac{\omega_m^{\frac{1}{3}}}{T(z)^{\frac{2}{3}}} \simeq \omega_m\left[1-1.19B(z)^{-\frac{2}{3}}\right],$$

and the broadened spectrum has a FWHM of

$$\omega_{FWHM}(z) = 2\omega_m. \quad (24)$$

To determine κ, we introduce normalized time $\tau = T/T_0$ and normalized length $Z = z/L_c$, and rewrite Eq. (7) as

$$i\frac{\partial U}{\partial Z} = \frac{1}{N}\frac{\partial^2 U}{\partial \tau^2} - \frac{N}{2}|U|^2U. \quad (25)$$

It shows that soliton number N determines the pulse evolution, and, therefore, κ should be a function of N. After careful comparison between analytical and simulation results, we find the following empirical formula:

$$\kappa = \begin{cases} 2.81 + \frac{\ln(N)}{26}, \beta_2>0 \quad (26) \\ 2.03 + \frac{\ln(N)}{8}, \beta_2<0 \quad (27) \end{cases} \quad (26)$$

Figure 3 shows that κ increases slowly with an increased N. More specifically, it increases from 2.9 (2.32) to 3.0 (2.65) as N increases from 10 to 150 for positive (negative) GVD.

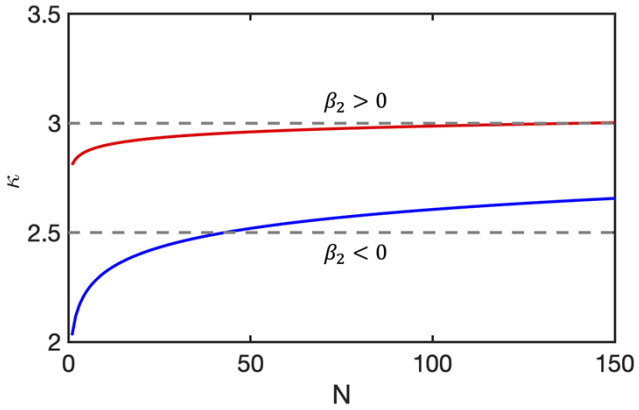

Fig. 3. κ versus N corresponding to an initial transform-limited Gaussian pulse propagating in fibers with positive (red curve) or negative (blue curve) GVD.

3.1.1. Spectral broadening of transform-limited Gaussian pulse with $\beta_2>0$

We first verify our analytical results for positive GVD. Figure 4 compares spectral evolution versus propagation distance given by numerical simulations [Fig. 4(a)] and by our analytical

Optics EXPRESS

solution [Fig. 4(b)] for $N = 60$ with $\beta_2>0$. Although significant difference exists between these two methods in terms of spectral structures, our analytical solution does provide a good prediction of the peak position of the OSLs. This is evidenced by the red and black line in Fig. 4(a), which indicate the normalized MIF $\omega_m T_0$ [Eq. (21)] and the OSL peak frequency $\omega_p T_0$ [Eq. (23)], respectively. For SPM-enabled spectral broadening in the positive GVD regime, the spectral bandwidth increases at the initial propagation, then reaches a maximum value, and decreases slowly due to optical wave-breaking for further propagation [18]. Our analytical results recover such a characteristic feature. As a comparison, the white line corresponds to the estimation of spectral broadening $\Delta\omega(z)$ given by Eq. (13) derived in Ref. [35], which predicts that the spectral bandwidth inreases monotonically along the propagtion.

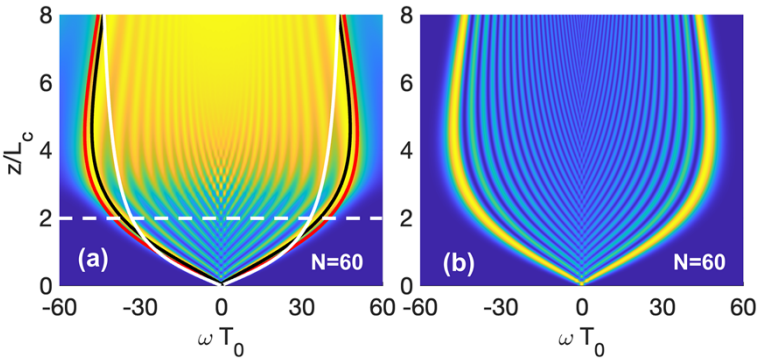

Fig. 4. Comparison of spectral evolution given by (a) numerical simulation and by (b) analytical solution [i.e., Fourier transform of Eq. (15)] for $N = 60$ and $\beta_2>0$. The red curve and black curve in (a) correspond to our analytical prediction of the MIF $\omega_m T_0$ and the OSL peak frequency $\omega_p T_0$; white solid curve represents the estimation of spectral broadening given by Eq. (13). The white dashed line marks the distance of $z = 2L_c$ for the onset of optical wave-breaking.

To make a detailed comparison, we choose the spectra in Fig. 4(a) at the propagation distances of L_c, $2L_c$, $3L_c$, $4L_c$, and $8L_c$, and plot them as black curves in Fig. 5. The red curves in this figure are the spectra [i.e., Fourier transform of Eq. (15)] in Fig. 4(b) at the same distances. The results indicate that the spectral evolution can be divided into the following stages:

(1) $z \le L_c$: The spectral broadening is dominated by SPM, which results in clearly separated spectral lobes. In this stage, the analytical results are in excellent agreement with the simulation results.

(2) $L_c<z \le 3L_c$: The positive GVD starts to play an important role and consequently the spectral lobes tend to gradually wash out. The deviation of the analytical results from the simulation results becomes larger for an increased propagation distance.

(3) (3) $3L_c<z \le 4L_c$: Although the onset of optical wave-breaking occurs at $z \simeq 2L_c$ according to Ref. [31], the resulting spectral pedestals start to appear at both sides of the spectrum for $z>3L_c$. Meanwhile, the shift of OSLs slows down and reaches a maximum value at $z \simeq 4L_c$.

(4) $z>4L_c$: The spectral lobes gradually merge together and the central portion of the broadened spectrum becomes top flattened. The two pedestals due to optical wave-breaking grow continuously in terms of both bandwidth and energy. The OSLs shift towards the spectral center and thus the central portion of the spectrum becomes narrower and flatter.

Optics EXPRESS

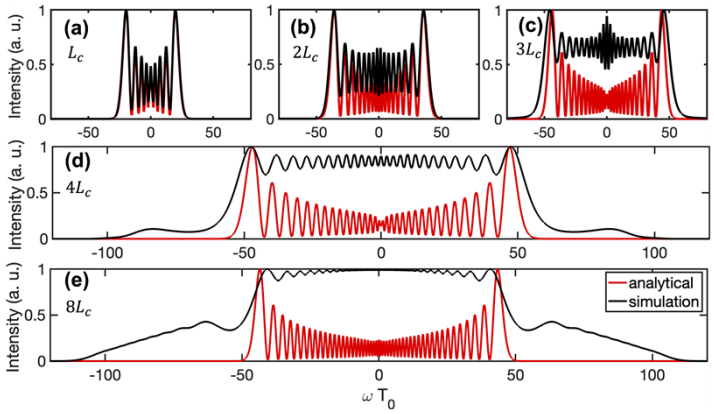

Fig. 5. Comparison of spectral evolution given by numerical simulation (black line) and by analytical solution (red line) at different distances: (a) $z = L_c$, (*b*) $z = 2L_c$, (*c*) $z = 3L_c$, (*d*)$z = 4L_c$, and (*e*) $z = 8L_c$ with $N = 60$, β_2>0.

Although our simple model does not recover the effect of optical wave-breaking, it does reasonably predict the OSL peak position and the spectral bandwidth. To make a direct comparison, we plot in Fig. 6(a) the OSL peak frequency as a function of the propagation distance for $N = 20$, 60, and 100. The solid squares represent the simulation results and the curves correspond to the analytical results given by Eq. (23). Figure 6(b) compares the spectral FWHM given by simulation results (solid squares) and by Eq. (24) (solid curves). The analytical expressions agree well with the simulation results.

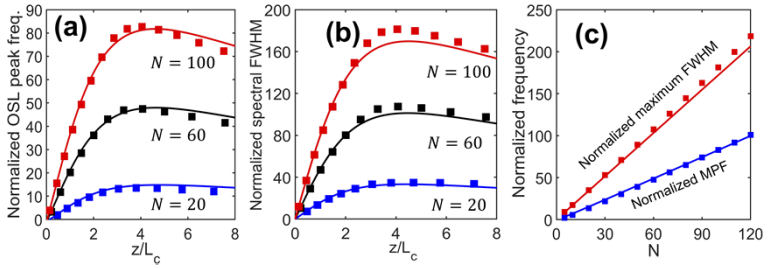

Fig. 6. (a) Normalized OSL peak frequency and (b) Normalized spectral FWHM as a function of the propagation distance for $N = 20$, 60, and 100 with β_2>0. (c) Normalized MPF and maximum FWHM versus N in the range between 5 and 120. Solid squares: simulation results; curves: analytical solutions .

For experimental designs, the maximum peak frequency (MPF) of the OSLs and the maximum FWHM are the two most important parameters. Extensive simulations show that these two maxima occur at the propagation distance of $4.0L_c$- $4.6L_c$ depending on the soliton number N. To estimate these values using our analytical results, we need to find the maximum values of Eq. (21) and Eq. (23). At $z \simeq 1.5\kappa L_c$, both functions reach the maximum value:

$$\omega_m^{max} \simeq \frac{\sqrt{2}e^{-\frac{1}{2}}\kappa N}{3T_0}, \tag{28}$$

$$\omega_p^{max} \simeq \frac{\sqrt{2}e^{-\frac{1}{2}}\kappa N}{3T_0}\left[1 - \frac{5}{3}(\kappa N)^{-\frac{2}{3}}\right]. \tag{29}$$

Optics EXPRESS

The maximum FWHM is given by

$$\omega_{FWHM}^{max} = 2\omega_m^{max} \simeq \frac{2\sqrt{2}e^{-\frac{1}{2}}\kappa N}{3T_0}. \tag{30}$$

Figure 3 shows that $\kappa \simeq 3$ for a big range of N, which further simplifies Eqs. (29)(30):

$$\omega_p^{max} \simeq \frac{\sqrt{2}e^{-\frac{1}{2}}N}{T_0}\left(1 - \frac{5}{3^{\frac{5}{3}}}N^{-\frac{2}{3}}\right) \simeq \frac{0.86N}{T_0}\left(1 - 0.8N^{-\frac{2}{3}}\right), \tag{31}$$

$$\omega_{FWHM}^{max} \simeq \frac{2\sqrt{2}e^{-\frac{1}{2}}N}{T_0} \simeq \frac{1.72N}{T_0}. \tag{32}$$

The blue curve in Fig. 6(c) shows the normalized MPF given by Eq. (31), which agrees well with the simulation results (solid squares). The red curve shows the estimation of the maximum FWHM using Eq. (32), which tends to deviate from the simulation results as N increases. For N larger than 50, Eq. (32) underestimates the FWHM with a deviation less than 5%.

3.1.2. Spectral broadening of transform-limited Gaussian pulse with $\beta_2<0$

To verify that our analytical results are valid for spectral broadening with $\beta_2<0$, we compare spectral evolution versus propagation distance given by numerical simulation [Fig. 7(a)] and by our analytical solution [Fig. 7(b)] for $N = 60$. Surprisingly, these two methods generate similar spectral structures with the propagation distance up to $z = 1.14L_c$, where the higher-order soliton experiences the maximum compression and reaches the minimum duration. In the following, we use L_{MC} to denote this distance. Further propagation beyond L_{MC} stretches the compressed pulse followed by generation of multi-soliton temporal structure and consequently the spectrum starts to develop complicated structures [27]. Chen and Kelley numerically found that $L_{MC} \simeq 1.82L_d/N$, which is equivalent to $L_{MC} \simeq 1.1L_c$ (white dotted line in Fig. 7) [33]. The red and black line in Fig. 7(a), which indicates the normalized MIF $\omega_m T_0$ [Eq. (22)] and the OSL peak frequency $\omega_p T_0$ [Eq. (23)], respectively. Clearly, our analytical solution provides a good prediction of the OSL peak position during the entire propagation stage of higher-order soliton self-compression. As a comparison, the white solid line in Fig. 7(a) corresponds to the estimation of spectral broadening $\Delta\omega(z)$ given by Eq. (14) that is derived in Ref. [35], which diverges at the distance of $z = L_c$ (white dashed line).

To make a detailed comparison, we choose the spectra in Fig. 7(a) at the propagation distances of $0.4L_c$, $0.6L_c$, $0.8L_c$, and $1.1L_c$, and plot them as black curves in Fig. 8. The red curves in this figure are the spectra in Fig. 7(b) at the same distances. The results indicate that, for $z \leq 0.6L_c$, the analytical results are in excellent agreement with the simulations. Further propagation leads to an increased deviation of the analytical results from the simulations. In contrast to the spectral washout that occurs in the positive-GVD case, negative GVD suppresses the intermediate lobes sitting between the two OSLs. In other words, these two OSLs contain larger portion of input pulse energy with an increased propagation distance up to $L_{MC} \simeq 1.1L_c$. For example, the two OSLs of the black curve in Fig. 8(d) contains 70% of pulse energy.

Figure 9(a, b) plot the normalized OSL peak frequency and the spectral FWHM as a function of propagation distance for $N = 20$, 60, and 100, respectively. The analytical solutions displayed as solid curves agree well with the simulation results represented by solid squares.

For negative GVD, it is more convenient to estimate the MPF at $L_{MC} \simeq 1.1L_c$. Plugging $z = 1.1L_c$ into Eq. (22) and Eq. (23) yields

$$\omega_m^{max} \simeq \frac{e^{-\frac{1}{2}}\kappa N}{\sqrt{2}T_0}\sin^{-1}\left(\frac{1.1}{k}\right)\left[1 - \frac{1.1^2}{k^2}\right]^{-\frac{1}{2}}, \tag{33}$$

Optics EXPRESS

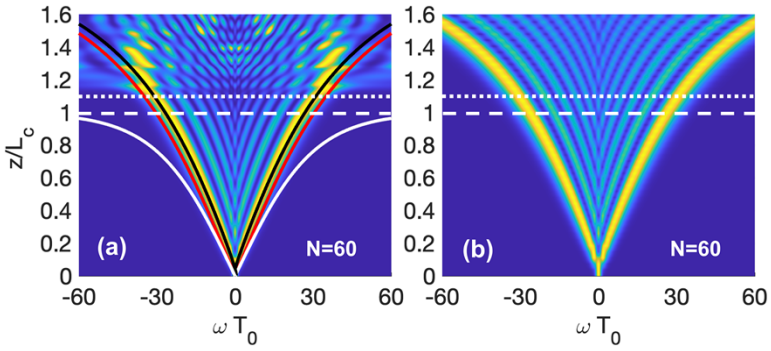

Fig. 7. Comparison of spectral evolution given by numerical simulation (a) and by analytical solution (b) for $N = 60$ and $\beta_2 < 0$. The red curve and black curve in (a) correspond to our analytical prediction of the MIF $\omega_m T_0$ and the OSL peak frequency $\omega_p T_0$; white solid curve represents the estimation of spectral broadening given by Eq. (14). The white dashed lines and white dotted lines mark the distance of z=L_c and z=1.1L_c, respectively.

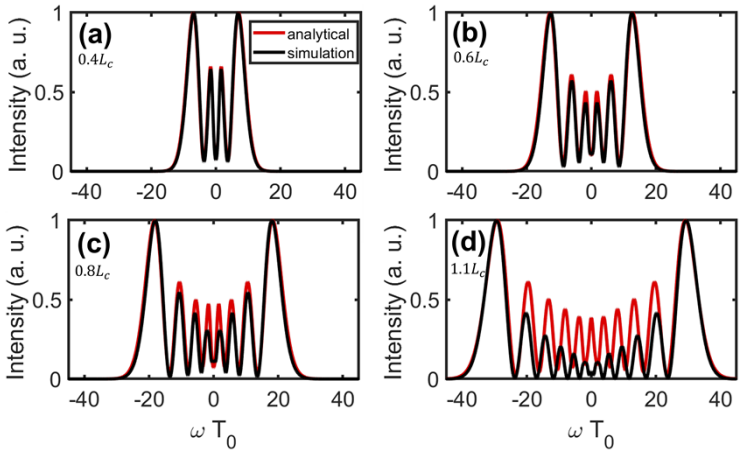

Fig. 8. Comparison of spectral evolution given by numerical simulation (black line) and by analytical solution (red line) at different distances: (a) $z = 0.4L_c$, (*b*) $z = 0.6L_c$, (*c*) $z = 0.8L_c$, and (*d*) $z = 1.1L_c$ with $N = 60$, $\beta_2 < 0$.

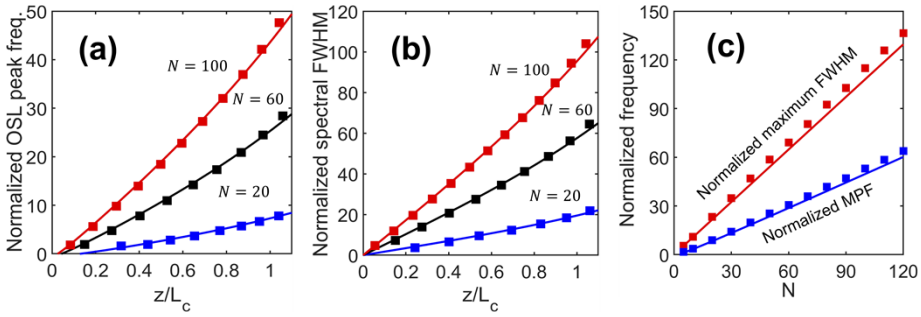

Fig. 9. (a) Normalized OSL peak frequency and (b) Normalized spectral FWHM as a function of the propagation distance for N = 20, 60, and 100 with $\beta_2 < 0$. (c) Normalized MPF and normalized maximum FWHM versus N in the range between 5 and 120. Squares: simulation results, solid curves: analytical solutions .

Optics EXPRESS

$$\omega_P^{max} \simeq \omega_m^{max}\left\{1-1.19\left[\frac{\kappa N}{2}\sin^{-1}\left(\frac{1.1}{k}\right)\right]^{-\frac{2}{3}}\right\}. \tag{34}$$

The maximum FWHM is then given by

$$\omega_{FWHM}^{max} = 2\omega_m^{max} \simeq \frac{\sqrt{2}e^{-\frac{1}{2}}\kappa N}{T_0}\sin^{-1}\left(\frac{1.1}{k}\right)\left[1-\frac{1.1^2}{k^2}\right]^{-\frac{1}{2}}. \tag{35}$$

Figure 3 shows that $\kappa \simeq 2.5$ for a big range of N, and we plug it into Eqs. (34)(35) for a further simplification:

$$\omega_p^{max} \simeq \frac{0.54N}{T_0}\left(1-1.73N^{-\frac{2}{3}}\right), \tag{36}$$

$$\omega_{FWHM}^{max} \simeq \frac{1.08N}{T_0}. \tag{37}$$

Figure 9(c) shows the MPF and maximum FWHM given by simulation and by Eq. (36)(37). Out analytical results slightly underestimate the MPF and FWHM with a deviation less than 5% as N varies between 5 and 120.

3.2. Spectral broadening of transform-limited hyperbolic-secant pulse

For an input transform-limited hyperbolic secant pulse, we use Eq. (5) to estimate the MIF:

$$\omega_m(z) = \frac{4B(z)}{3\sqrt{3}T(z)} = \begin{cases} \frac{2\kappa N}{3\sqrt{3}T_0}\sinh^{-1}\left(\frac{z}{\kappa L_c}\right)\left[1+\frac{z^2}{(\kappa L_c)^2}\right]^{-\frac{1}{2}}, \ \beta_2>0 & (38) \\ \frac{2\kappa N}{3\sqrt{3}T_0}\sin^{-1}\left(\frac{z}{\kappa L_c}\right)\left[1-\frac{z^2}{(\kappa L_c)^2}\right]^{-\frac{1}{2}}, \ \beta_2<0 & (39) \end{cases}$$

We can then estimate the OSL peak frequency following Eq. (6) and the FWHM of the broadened spectrum:

$$\omega_P(z) \simeq \omega_m - \frac{\pi^{\frac{2}{3}}}{2}\frac{\omega_m^{\frac{1}{3}}}{T(z)^{\frac{2}{3}}} \simeq \omega_m\left[1-1.28B(z)^{-\frac{2}{3}}\right], \tag{40}$$

$$\omega_{FWHM} = 2\omega_m. \tag{41}$$

For hyperbolic secant pulse, we find the following empirical formula for κ:

$$\kappa = \begin{cases} 2.54+\frac{\ln(N)}{6.5}, \ \beta_2>0 & (42) \\ 1.87+\frac{\ln(N)}{18}, \beta_2<0 & (43) \end{cases}$$

Figure 10 shows that κ increases slowly from 2.9 (2.0) to 3.3 (2.15) for positive (negative) GVD as N increases from 10 to 150.

We first discuss the case for $\beta_2>0$. To estimate the OSL MPF and the maximum spectral FWHM, we need to find the maximum values of Eq. (40) and Eq. (41). At $z \simeq 1.5\kappa L_c$, both

Optics EXPRESS

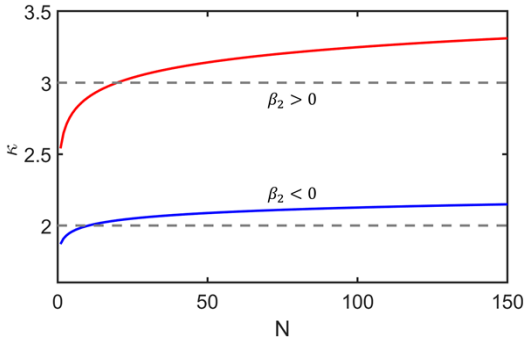

Fig. 10. κ versus N corresponding to an initial transform-limited hyperbolic-secant pulse propagating in fibers with positive (red curve) GVD or negative (blue curve) GVD.

functions reach the maximum value:

$$\omega_P^{max} \simeq \frac{4\kappa N}{9\sqrt{3}T_0}\left[1 - 1.8(\kappa N)^{-\frac{2}{3}}\right], \tag{44}$$

$$\omega_{FWHM}^{max} \simeq \frac{8\kappa N}{9\sqrt{3}T_0}. \tag{45}$$

The red curve in Fig. 10 shows that $\kappa \simeq 3.2$ for a big range of N, resulting in further simplification:

$$\omega_P^{max} \simeq \frac{0.82N}{T_0}\left(1 - 0.83N^{-\frac{2}{3}}\right), \tag{46}$$

$$\omega_{FWHM}^{max} \simeq \frac{1.64N}{T_0}. \tag{47}$$

For hyperbolic secant pulse propagating inside an optical fiber with β_2<0, Chen and Kelley numerically found that $L_{MC} \simeq 1.93L_d/N$, which is equivalent to $L_{MC} \simeq 1.03L_c \simeq 1L_c$ [33]. Plugging z = L_c into Eq. (39) and Eq. (40) yields

$$\omega_m^{max} \simeq \frac{2\kappa N}{3\sqrt{3}T_0}\sin^{-1}\left(\frac{1}{k}\right)\left[1 - \frac{1}{k^2}\right]^{-\frac{1}{2}}, \tag{48}$$

$$\omega_P^{max} \simeq \omega_m^{max}\left\{1 - 1.28\left[\frac{\kappa N}{2}\sin^{-1}\left(\frac{1}{k}\right)\right]^{-\frac{2}{3}}\right\}. \tag{49}$$

The maximum FWHM is then given by

$$\omega_{FWHM}^{max} = 2\omega_m^{max} \simeq \frac{4\kappa N}{3\sqrt{3}T_0}\sin^{-1}\left(\frac{1}{k}\right)\left[1 - \frac{1}{k^2}\right]^{-\frac{1}{2}}. \tag{50}$$

The blue curve in Fig. 10 shows that $\kappa \simeq 2.1$ for N in a big range, which further simplifies Eqs. (49)(50):

$$\omega_p^{max} \simeq \frac{0.46N}{T_0}\left(1 - 1.98N^{-\frac{2}{3}}\right), \tag{51}$$

$$\omega_{FWHM}^{max} \simeq \frac{0.91N}{T_0}. \tag{52}$$

Figure 11 shows both the simulation results (solid squares) and analytical solutions (solid curves) for the normalized OSL peak frequency [Fig. 11(a)] and spectral FWHM [Fig. 11(b)] as

Optics EXPRESS

a function of the propagation distance for $N = 20$, 60, and 100, respectively, for $\beta_2 > 0$; Fig. 11(c) shows the MPF and maximum FWHM given by simulation and by Eq. (46)(47). Figure (d-f) present a similar comparison as Fig. 11(a-c) for the case of $\beta_2 < 0$. The results clearly indicate the excellent agreement between analytical solutions and simulation results.

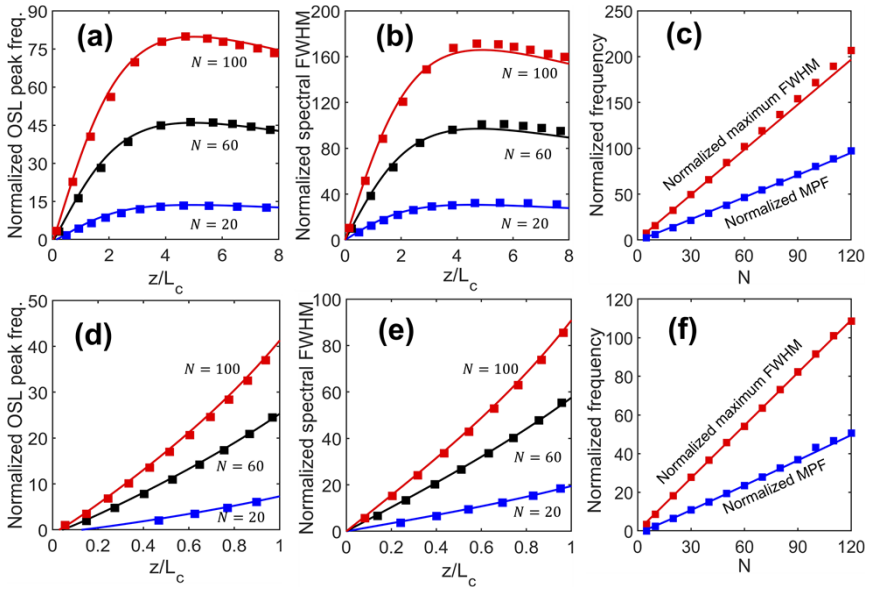

Fig. 11. Comparison between simulation results and analytical solutions for hyperbolic secant pulse propagating in fibers with different GVD sign: (a-c) $\beta_2 > 0$ and (d-f) $\beta_2 < 0$. (a, d) Normalized OSL peak frequency and (b, e) Normalized spectral FWHM as a function of propagation distance for $N = 20$, 60, and 100. (c, f) Normalized MPF and normalized maximum FWHM versus N in the range between 5 and 120. Solid squares: simulation results, solid curves: analytical solutions .

4. Discussion and conclusion

Table 1 summarizes the unified analytical solutions for a Gaussian or Sech input pulse propagating in the strong nonlinearity regime with either positive or negative GVD. The results seem to suggest that reducing the input pulse duration T_0 can efficiently increase the FWHM of the broadened spectrum since ω_{FWHM}^{max} is proportional to N/T_0. Indeed, given that $N = \sqrt{L_d/L_{NL}} = T_0\sqrt{\gamma P_0/\beta_2}$, $\omega_{FWHM}^{max} \sim \sqrt{\gamma P_0/\beta_2}$ and is independent on pulse duration. In another word, the maximum bandwidth is only determined by fiber nonlinear parameter, GVD, and pulse peak power. This has important implication on the application that demands maximizing the spectral bandwidth of the broadened spectrum such as low-noise continuum generation, nonlinear pulse compression, and SESS.

Our results provide useful guidelines for choosing proper experimental parameters to optimize the SPM-enabled spectral broadening. For example, implementation of a SESS source prefers a broadened spectrum with well-separated spectral lobes to ensure high conversion efficiency and minimized noise [36]. If the fiber has negative GVD, the broadened spectrum always consists of isolated spectral lobes as long as the fiber length is shorter than L_{MC}, which is about $1.1L_c$ (L_c) for Gaussian (Sech) input pulse. As the fiber has positive GVD, the fiber length is better less than $2L_c$ to prevent optical wave-breaking and maintain clear spectral lobes. Our solutions predict the peak position of the OSLs, which after filtering corresponds the peak wavelength of

Optics EXPRESS

Table 1. Main analytical results on estimation of SPM-enabled spectral broadening for Gaussian or hyperbolic secant pulse propagating inside optical fibers with positive or negative GVD

	$\beta_2>0$		$\beta_2<0$	
	Gaussian	Sech	Gaussian	Sech
$\kappa = \alpha + \frac{\log(N)}{\beta}$	$\alpha = 2.81$ $\beta = 26$	$\alpha = 2.54$ $\beta = 6.5$	$\alpha = 2.03$ $\beta = 8$	$\alpha = 1.87$ $\beta = 18$
$T(z) = T_0[1 + \alpha\frac{z^2}{(\kappa L_c)^2}]^{\frac{1}{2}}$	$\alpha = +1$		$\alpha = -1$	
$B(z) = \frac{\kappa N}{2} f(z)$	$f(z) = \sinh^{-1}(\frac{z}{\kappa L_c})$		$f(z) = \sin^{-1}(\frac{z}{\kappa L_c})$	
$\omega_m(z) = \alpha\frac{B(z)}{T(z)}$	$\alpha = \sqrt{2}e^{-\frac{1}{2}}$	$\alpha = \frac{4}{3\sqrt{3}}$	$\alpha = \sqrt{2}e^{-\frac{1}{2}}$	$\alpha = \frac{4}{3\sqrt{3}}$
$\omega_P(z) \simeq \omega_m[1 - \beta B(z)^{-\frac{2}{3}}]$	$\beta = 1.19$	$\beta = 1.28$	$\beta = 1.19$	$\beta = 1.28$
$\omega_{FWHM}(z) = 2\omega_m(z)$	$2\omega_m(z)$			
$\omega_P^{max} \simeq \alpha\frac{N}{T_0}(1 - \beta N^{-\frac{2}{3}})$	$\alpha = 0.86$ $\beta = 0.8$	$\alpha = 0.82$ $\beta = 0.8_3$	$\alpha = 0.54$ $\beta = 1.73$	$\alpha = 0.46$ $\beta = 1.98$
$\omega_{FWHM}^{max} \simeq \alpha\frac{N}{T_0}$	$\alpha = 1.72$	$\alpha = 1.64$	$\alpha = 1.08$	$\alpha = 0.91$

the filtered SESS pulses. In other words, we can use these analytical results to quickly design the experimental parameters in order to achieve a SESS pulse at a targeted wavelength.

In recent years, the combination of SPM-enabled spectral broadening and bandpass filters constitutes an effective saturable absorber in Mamyshev oscillators—a new type of passively mode-locked oscillators that are immune to environmental disturbance and can deliver μJ-level pulse energy [37–40]. Our analytical results may provide some insight when designing these oscillators. Mamyshev oscillators that produce high peak-power femtosecond pulses at 1.03 μm, 1.55 μm, and 2.0 μm have been demonstrated by incorporating Yb-fiber, Er-fiber, and Tm-fiber into the laser cavity, respectively [37,38,41–43]. In all the reported Mamyshev oscillators, fibers with positive GVD were employed to facilitate SPM-enabled spectral broadening. Our work in this paper indicates that SPM together with negative GVD can efficiently broaden the spectrum prior to the pulse splitting that occurs after reaching the maximum soliton self-compression. We anticipate that Mamyshev oscillators operating at 1.55 μm or 2.0 μm can be constructed using all negative-GVD fibers, which may further improve the energy scalability.

To conclude, we present an analytical treatment of fiber-optic spectral broadening resulting from SPM and GVD by solving the NLSE in the strong nonlinearity (i.e., $L_{NL} \ll L_d$) regime. To quantify the OSL peak frequency of the broadened spectrum, we extend the work by Finot *et al.* [i.e., Ref. (26)] that analyzed the spectral broadening due to pure SPM. As shown by Eqs. (3-6), they first calculated MIF, ω_m, which is proportional to the ratio between B integral and pulse duration; then they further expressed the OSL peak frequency, ω_P, as a function of ω_m [26]. In this paper, we generalize Eqs. (3-6) to the scenario that GVD is taken into account, and thus the most important step is to find the expression for the z-dependent pulse duration and B integral. Inspired by Zheltikov's work [i.e., Ref. (35)] that defined a lumped chirp parameter α_0 to account for SPM when estimating the pulse duration in the strong nonlinearity regime, we modify α_0 by including κ—a fitting parameter determined by matching the simulation results with the analytical solutions. We further calculate the z-dependence B integral, and then obtain the closed-form analytical solutions for MIF ω_m and the OSL peak frequency ω_P. We also demonstrate that the FWHM of the broadened spectrum is well estimated by $2\omega_m$. These analytical solutions allow us to identify the maximum values of the OSL peak frequency and the spectral FWHM. In this paper, we present the unified results for both Gaussian and hyperbolic secant pulse as the input. Given that Ref. [26] also obtained analytical results for spectral broadening by pure

Optics EXPRESS

SPM for Lorentzian and super-Gaussian pulse, we believe that our method can be applied to these two pulse shapes as well. Our findings provide useful insights for experiments that involve optimization of the SPM-enabled spectral broadening such as nonlinear compression of relatively long pulses, design of SESS sources, implementation of pulse regenerators, and construction of Mamyshev oscillators.

Funding. National Natural Science Foundation of China (No. 62175255); National Key Research and Development Program of China (No. 2021YFB3602602); Chinese Academy of Sciences (YJKYYQ20190034).

Acknowledgment. We thank Professor Zhiyi Wei for useful discussions.

During the revision, we noticed a conference presentation that employed the results in Ref. [26] to analyze the peak position and bandwidth of the OSLs of experimentally obtained spectra broadened mainly by SPM [44].

Disclosures. The authors declare no conflicts of interest.

Data availability. Data underlying the results presented in this paper are not publicly available at this time but may be obtained from the authors upon reasonable request.

References

1. R. H. Stolen and C. Lin, "Self-phase-modulation in silica optical fibers," Phys. Rev. A **17**(4), 1448–1453 (1978).
2. H. Nakatsuka, D. Grischkowsky, and A. C. Balant, "Nonlinear Picosecond-Pulse Propagation through Optical Fibers with Positive Group Velocity Dispersion," Phys. Rev. Lett. **47**(13), 910–913 (1981).
3. W. J. Tomlinson, R. H. Stolen, and C. V. Shank, "Compression of optical pulses chirped by self-phase modulation in fibers," J. Opt. Soc. Am. B **1**(2), 139–149 (1984).
4. C. V. Shank, R. L. Fork, R. Yen, R. H. Stolen, and W. J. Tomlinson, "Compression of femtosecond optical pulses," Appl. Phys. Lett. **40**(9), 761–763 (1982).
5. L. F. Mollenauer, R. H. Stolen, J. P. Gordon, and W. J. Tomlinson, "Extreme picosecond pulse narrowing by means of soliton effect in single-mode optical fibers," Opt. Lett. **8**(5), 289–291 (1983).
6. P. V. Mamyshev, "All-optical data regeneration based on self-phase modulation effect," in *24th European Conference on Optical Communication. ECOC '98 (IEEE Cat. No.98TH8398)* (1998), 1, pp. 475–476 vol.1.
7. T.-H. Her, G. Raybon, and C. Headley, "Optimization of pulse regeneration at 40 Gb/s based on spectral filtering of self-phase modulation in fiber," IEEE Photonics Technol. Lett. **16**(1), 200–202 (2004).
8. L. B. Fu, M. Rochette, V. G. Ta'eed, D. J. Moss, and B. J. Eggleton, "Investigation of self-phase modulation based optical regeneration in single mode As_2Se_3 chalcogenide glass fiber," Opt. Express **13**(19), 7637–7644 (2005).
9. R. Lehneis, A. Steinmetz, J. Limpert, and A. Tünnermann, "All-fiber pulse shortening of passively Q-switched microchip laser pulses down to sub-200 fs," Opt. Lett. **39**(20), 5806–5809 (2014).
10. W. Fu, L. G. Wright, and F. W. Wise, "High-power femtosecond pulses without a modelocked laser," Optica **4**(7), 831–834 (2017).
11. J. Buldt, M. Müller, R. Klas, T. Eidam, J. Limpert, and A. Tünnermann, "Temporal contrast enhancement of energetic laser pulses by filtered self-phase-modulation-broadened spectra," Opt. Lett. **42**(19), 3761–3764 (2017).
12. M. Närhi, A. Fedotov, K. Aksenova, J. Fiebrandt, T. Schönau, M. Gerecke, and R. Gumenyuk, "Design guidelines for ultrashort pulse generation by a Mamyshev regenerator," Opt. Express **29**(10), 15699–15710 (2021).
13. C. Finot and J. Fatome, "All-optical fiber-based ultrafast amplitude jitter magnifier," Opt. Express **18**(18), 18697–18702 (2010).
14. C. H. Lin and T. K. Gustafson, "Optical Pulsewidth Measurement Using Self-Phase Modulation," IEEE J. Quantum Electron. **8**(4), 429–430 (1972).
15. K. Baudin, F. Audo, and C. Finot, "Fiber-based measurement of temporal intensity and phase profiles of an optical telecommunication pulse through self-phase modulation," Microw. Opt. Technol. Lett. **60**(4), 882–886 (2018).
16. Y. Liu, H. Tu, and S. A. Boppart, "Wave-breaking-extended fiber supercontinuum generation for high compression ratio transform-limited pulse compression," Opt. Lett. **37**(12), 2172–2174 (2012).
17. D. Castelló-Lurbe, N. Vermeulen, and E. Silvestre, "Towards an analytical framework for tailoring supercontinuum generation," Opt. Express **24**(23), 26629–26645 (2016).
18. C. Finot, B. Kibler, L. Provost, and S. Wabnitz, "Beneficial impact of wave-breaking for coherent continuum formation in normally dispersive nonlinear fibers," J. Opt. Soc. Am. B **25**(11), 1938–1948 (2008).
19. A. M. Heidt, A. Hartung, G. W. Bosman, P. Krok, E. G. Rohwer, H. Schwoerer, and H. Bartelt, "Coherent octave spanning near-infrared and visible supercontinuum generation in all-normal dispersion photonic crystal fibers," Opt. Express **19**(4), 3775–3787 (2011).
20. L. E. Hooper, P. J. Mosley, A. C. Muir, W. J. Wadsworth, and J. C. Knight, "Coherent supercontinuum generation in photonic crystal fiber with all-normal group velocity dispersion," Opt. Express **19**(6), 4902–4907 (2011).
21. A. Rampur, D.-M. Spangenberg, B. Sierro, P. Hänzi, M. Klimczak, and A. M. Heidt, "Perspective on the next generation of ultra-low noise fiber supercontinuum sources and their emerging applications in spectroscopy, imaging, and ultrafast photonics," Appl. Phys. Lett. **118**(24), 240504 (2021).
22. W. Liu, C. Li, Z. Zhang, F. X. Kärtner, and G. Chang, "Self-phase modulation enabled, wavelength-tunable ultrafast fiber laser sources: an energy scalable approach," Opt. Express **24**(14), 15328–15340 (2016).

Optics EXPRESS

23. H.-Y. Chung, W. Liu, Q. Cao, F. X. Kärtner, and G. Chang, "Er-fiber laser enabled, energy scalable femtosecond source tunable from 13 to 17 μm," Opt. Express **25**(14), 15760–15771 (2017).
24. H.-Y. Chung, W. Liu, Q. Cao, L. Song, F. X. Kärtner, and G. Chang, "Megawatt peak power tunable femtosecond source based on self-phase modulation enabled spectral selection," Opt. Express **26**(3), 3684–3695 (2018).
25. X. Diao, R. Chen, and G. Chang, "Particle swarm optimization of SPM-enabled spectral selection to achieve an octave-spanning wavelength-shift," Opt. Express **29**(24), 39766–39776 (2021).
26. C. Finot, F. Chaussard, and S. Boscolo, "Simple guidelines to predict self-phase modulation patterns," J. Opt. Soc. Am. B **35**(12), 3143–3152 (2018).
27. G. P. Agrawal, *Nonlinear Fiber Optics*, Sixth edition (Academic, 2019).
28. M. J. Potasek, G. P. Agrawal, and S. C. Pinault, "Analytic and numerical study of pulse broadening in nonlinear dispersive optical fibers," J. Opt. Soc. Am. B **3**(2), 205–211 (1986).
29. C. Pask and A. Vatarescu, "Spectral approach to pulse propagation in a dispersive nonlinear medium," J. Opt. Soc. Am. B **3**(7), 1018–1024 (1986).
30. D. Marcuse, "RMS width of pulses in nonlinear dispersive fibers," J. Lightwave Technol. **10**(1), 17–21 (1992).
31. D. Anderson, M. Desaix, M. Lisak, and M. L. Quiroga-Teixeiro, "Wave breaking in nonlinear-optical fibers," J. Opt. Soc. Am. B **9**(8), 1358–1361 (1992).
32. S. Taccheo and L. Boivin, "Investigation and design rules of supercontinuum sources for WDM applications," in *Optical Fiber Communication Conference. Technical Digest Postconference Edition. Trends in Optics and Photonics Vol.37 (IEEE Cat. No. 00CH37079)* (Opt. Soc. America, 2000), 3, pp. 2–4.
33. C.-M. Chen and P. L. Kelley, "Nonlinear pulse compression in optical fibers: scaling laws and numerical analysis," J. Opt. Soc. Am. B **19**(9), 1961–1967 (2002).
34. C.-J. Rosenberg, D. Anderson, M. Desaix, P. Johannisson, and M. Lisak, "Evolution of optical pulses towards wave breaking in highly nonlinear fibres," Opt. Commun. **273**(1), 272–277 (2007).
35. A. Zheltikov, "Analytical insights into self-phase modulation: beyond the basic theory," Opt. Express **26**(13), 17571–17577 (2018).
36. Y. Hua, G. Zhou, W. Liu, M. Xin, F. X. Kärtner, and G. Chang, "Femtosecond two-color source synchronized at 100-as-precision based on SPM-enabled spectral selection," Opt. Lett. **45**(13), 3410–3413 (2020).
37. P. Sidorenko, W. Fu, L. G. Wright, M. Olivier, and F. W. Wise, "Self-seeded, multi-megawatt, Mamyshev oscillator," Opt. Lett. **43**(11), 2672–2675 (2018).
38. P. Repgen, D. Wandt, U. Morgner, J. Neumann, and D. Kracht, "Sub-50 fs, μJ-level pulses from a Mamyshev oscillator–amplifier system," Opt. Lett. **44**(24), 5973–5976 (2019).
39. T. Wang, B. Ren, C. Li, J. Wu, R. Su, P. Ma, Z.-C. Luo, and P. Zhou, "Over 80 nJ Sub-100 fs All-Fiber Mamyshev Oscillator," IEEE J. Sel. Top. Quantum Electron. **27**(6), 1–5 (2021).
40. W. Liu, R. Liao, J. Zhao, J. Cui, Y. Song, C. Wang, and M. Hu, "Femtosecond Mamyshev oscillator with 10-MW-level peak power," Optica **6**(2), 194–197 (2019).
41. M. Rochette, L. R. Chen, K. Sun, and J. Hernandez-Cordero, "Multiwavelength and Tunable Self-Pulsating Fiber Cavity Based on Regenerative SPM Spectral Broadening and Filtering," IEEE Photonics Technol. Lett. **20**(17), 1497–1499 (2008).
42. M. Olivier, V. Boulanger, F. Guilbert-Savary, P. Sidorenko, F. W. Wise, and M. Piché, "Femtosecond fiber Mamyshev oscillator at 1550 nm," Opt. Lett. **44**(4), 851–854 (2019).
43. P. Repgen, B. Schuhbauer, M. Hinkelmann, D. Wandt, A. Wienke, U. Morgner, J. Neumann, and D. Kracht, "Mode-locked pulses from a Thulium-doped fiber Mamyshev oscillator," Opt. Express **28**(9), 13837–13844 (2020).
44. L.-T. Chou and S.-H. Chia, "Widely Tunable Femtosecond Sources with Continuously Tailorable Bandwidth Enabled by Self-Phase Modulation," in *Conference on Lasers and Electro-Optics* (Optical Society of America, 2022), paper JW3B.119.